

Near-Infrared Observations of the Massive Star Forming Region IRAS 23151+5912*

Xue-Peng Chen and Yong-Qiang Yao

Purple Mountain Observatory, Chinese Academy of Sciences, Nanjing 210008; xpchen@pmo.ac.cn

Received 2003 June 5; accepted 2004 January 5

Abstract Near-infrared images and K-band spectroscopy of the massive star-forming region IRAS 23151+5912 are presented. The JHK' images reveal an embedded infrared cluster associated with infrared nebula, and the H₂ (2.12 μm) narrow-band image provides for the first time evidence of outflow activity associated with the cluster. That the cluster is young can be shown by the high percentage of infrared excess sources and the outflow activity. We suggest an age of the cluster of $\sim 10^6$ yr. Eight young stars are found in the bright nebular core around IRAS 23151+5912. By the color-magnitude diagrams of the cluster, we found five high-mass YSOs and four intermediate-mass YSOs in the cluster. Eight H₂ emission features are discovered in the region with a scattered and non-axisymmetric distribution, indicating the existence of multiple outflows driven by the cluster. Diffuse H₂ emission detected to the north and to the west of the cluster may result from UV leakage of the cluster. Brγ, H₂, and CIV emission lines are found in the K-band spectrum of the brightest source, NIRS 19, indicating the presence of envelope, stellar wind, and shock in the circumstellar environment. We have estimated an O7–O9 spectral type for the central massive YSO ($20 \sim 30M_{\odot}$), with an age of less than 1×10^6 yr.

Key words: infrared radiation — stars: formation: — ISM: individual: IRAS 23151 + 5912 — ISM: jets and outflows

1 INTRODUCTION

IRAS 23151+5912, located in the constellation Cepheus at a distance of 3.5 kpc, is well-known as a site of massive star formation (Cesaroni et al. 1999). The far infrared luminosity of the source has been estimated to be $3.9 \times 10^4 L_{\odot}$ (Wouterloot et al. 1989). As one sign of massive star formation, there is H₂O maser emission in the region, which is extensively studied (Wouterloot & Walmsley 1986; Scalise et al. 1989; Felli et al. 1992; Tofani et al. 1995). Two maser spots were detected with VLA observations located within 2'' of the IRAS position, and aligned in the NE–SW direction (Tofani et al. 1995). Although Tofani et al. detected no continuum emission in their 3.5 cm VLA map, Miralles et al. (1994) reported a radio source

* Supported by the National Natural Science Foundation of China.

toward IRAS 23151 at 2 cm and 6 cm. Recently, Beuther et al. (2002) found a peak in 1.2 mm dust continuum emission coincident with the IRAS 23151 position.

The molecular cloud core in IRAS 23151 has been observed to be $\sim 40''$ (0.6 pc) with the NH_3 (1, 1) line (Wouterloot et al. 1988). The CO observations display a NE–SW oriented molecular outflow, with $200 M_\odot$ outflow mass (Wouterloot et al. 1989). Cesaroni et al. (1999) has extensively observed IRAS 23151 with the C^{34}S , ^{13}CO , CS, HCO^+ (1–0), and HCN (1–0) molecular lines. For the two velocity peaks of the HCO^+ (1–0) and HCN (1–0) spectra, Cesaroni et al. (1999) suggested two molecular clumps in the cloud. Beuther et al. (2002) have observed the region again with the CS and C^{34}S lines, obtaining consistent results with Cesaroni et al. (1999).

Near-infrared observations are a powerful tool for understanding star formation and early evolution of dense molecular clouds. Near-infrared images of high angular resolution and large spatial coverage allow identification of the driving sources of outflows and masers and a complete census of young stellar populations. In the K-band survey of Hodapp (1994), bright infrared nebula was found in IRAS 23151 at the position of the outflow, but there were no detailed studies. In this paper, we present our near-infrared images toward IRAS 23151 in the JHK' broad bands and the $\text{H}_2 v = 1 - 0 \text{S}(1)$ narrow band, and our K-band spectroscopy from 2.0 to $2.35 \mu\text{m}$ of the NIR peak of IRAS 23151. Our observations reveal an embedded cluster associated with infrared nebula, and allow us to investigate the cluster properties, the nebular structure, and the outflow activity. The moderate-resolution spectrometry offers for the first time physical information about the massive young star in IRAS 23151. We describe in Sect. 2 the observations and present the results in Sect. 3. The observational results are discussed in Sect. 4 and summarized in Sect. 5.

2 OBSERVATIONS

2.1 Near-Infrared Imaging

The near-infrared images were taken with the 1.88 m telescope of Okayama Astronomical Observatory on 1999 November 3, with the infrared camera OASIS (Okayama Astrophysical System for Infrared imaging and Spectroscopy; Okumura et al. 2000). OASIS, equipped with a NICMOS3 array, provides a field of $4.2 \times 4.2 \text{ arcmin}^2$ with a plate scale of $0.97'' \text{ pixel}^{-1}$. Five dithered images were obtained with the J, H, and $\text{H}_2 v = 1 - 0 \text{S}(1)$ ($2.12 \mu\text{m}$) filters and 10 dithered images with the K' ($2.16 \mu\text{m}$) filter. Total integration times of 150, 50, 50, 300 s were taken for the J, H, K', and H_2 bands. The FWHM of the seeing disk was measured to be $\sim 1.8''$ during the observations.

The images were reduced with the IRAF package. Every image was dark-subtracted, flat-fielded, and background-subtracted. The flat field was constructed by two sets of dome flat frames taken by an illuminating lamp on and off. The background frames were obtained by median filtering of the flat-fielded data frames. The reduced images in each band were registered and aligned using common stars and then combined into a final image. To obtain an H_2 emission-line image, we subtracted a continuum image from the observed H_2 image. A weighted K' image was employed as the continuum image. The weighting factor is a median of the H_2 and K' flux ratios of field stars that are believed to have no H_2 line emission.

2.2 K-Band Spectroscopy

The spectra of IRAS 23151 were obtained on 2000 November 24 with OASIS. The spectral resolution of OASIS was set to be $\lambda/\Delta\lambda \sim 500$ with a 300 mm^{-1} grating and a $2.4''$ slit. The

wavelength coverage was from $2.0\ \mu\text{m}$ to $2.35\ \mu\text{m}$. The slit was about $230''$ long and was aligned roughly along the east-west direction. In the observations, the slit was centered on the K-band peak of IRAS 23151. The object was observed six times with the telescope dithered along the slit to reduce the effects of bad pixels and cosmic rays. Each exposure time was 3 minutes, and the telescope was guided during the exposure by monitoring nearby optically visible star with the slit-viewer of the camera. Standard stars were also observed for atmospheric correction and flux calibration. The seeing condition during the observations was $\sim 1.8''$.

Each spectrum frame was dark-subtracted and flat-fielded. The flat field was constructed by two sets of dome flat frames taken with an illuminating lamp on and off. The spectra were extracted using the IRAF APALL task. The extracted spectra were then level-adjusted with each other and median combined to produce a final spectrum. The spectrum was further divided by A0 V standard star (HR 9019) reduced in the same manner to remove atmospheric absorption features; $\text{Br}\gamma$ absorption in the A0 V standard has been removed with the SPLOT task after being divided by the late-type standard (HR 9079), which shows little $\text{Br}\gamma$ absorption (Wallace & Hinkle 1997). The spectrum was finally multiplied by a Planck function of an 9790 K blackbody, representative of the A0 V star. The accuracy of flux level was estimated to be $\sim 20\%$ from the change of signals obtained at different slit positions.

3 RESULTS

Figure 1 shows the near-infrared color image and the corresponding optical POSS image of IRAS 23151 in a field of $3.4' \times 4.2'$. The color image reveals an embedded small cluster associated with a bright infrared nebula, not detected in the optical. The color image shows that there are more point sources observed in the near-infrared bands than in the optical observation. The shape of the bright near-infrared nebula is roughly round, with a bright nebular core and a bright star in the center. Some juts can be seen to the east and southeast of the core. In Fig. 1b,

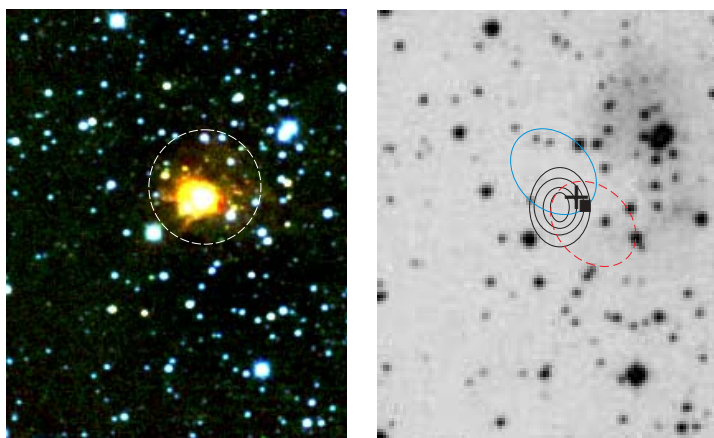


FIG. 1a

FIG. 1b

Fig. 1 JHK' linear-scale color image (left) and the corresponding optical image (right) of IRAS 23151. The field of view is $3.2' \times 4.2'$. Circle in the color image outlines the area of the infrared cluster. The cross, square, and contours in the optical image mark the positions of the IRAS source, H_2O maser, and molecular core, respectively. The blue solid line and red dash line delineate the blueshifted and redshifted CO outflow in the region.

there is a small optical nebula with two visible stars to the northwest of the infrared nebula. The optical nebula is very diffuse on a large scale and is nearly transparent in the near-infrared bands.

The JHK' photometry was carried out for the point sources in the observed field, using the IRAF DAOPHOT package. The photometric calibration was made with the standard stars in NGC 7790, AS40 (Hunt et al. 1998) observed on the same night. Discounting fake stars at the edge of the field background noise is high, we have detected 352, 310, and 257 sources in the J, H, and K' bands, respectively, in the whole $3.4' \times 4.2'$ field. The limiting magnitudes are 18.4, 16.8, and 16.1 mag, respectively, for the JHK' bands with uncertainties of 0.1 mag.

A close view of the infrared nebula area is shown by the JHK' contours and color image in Fig. 2. The maps are plotted with co-ordinates offset from the astrometry origin ($\alpha=23^{\text{h}}15^{\text{m}}05.55^{\text{s}}$, $\delta=+59^{\circ}12' 24.2''$, 1950.0; NIRS 33 in Table 1) with an accuracy of $\sim 1''$. We detected 37 point sources within a $\sim 70''$ (~ 1 pc) area of IRAS 23151, which encloses a cluster of red point sources in the nebular region. The positions and JHK' magnitudes of these point sources are listed in Table 1.

Table 1 Photometry of Near-infrared Point Sources in the Nebular Region

NIRS	$\Delta\alpha^{\text{a}}$ ($''$)	$\Delta\delta^{\text{a}}$ ($''$)	K' (mag)	[H-K']	[J-H]	NIRS	$\Delta\alpha^{\text{a}}$ ($''$)	$\Delta\delta^{\text{a}}$ ($''$)	K' (mag)	[H-K']	[J-H]
1	36.5	9.5	12.2	4.2	1.8	21	59.6	21.5	15.7	1.1	1.5
2	33.5	-1.1	10.6	3.9	2.3	22	60.0	-0.6	15.2	1.1	1.6
3	41.4	-11.6	14.1	3.9	1.3	23	29.5	25.8	15.3	1.0	2.3
4	29.4	-1.4	10.0	2.4	1.5	24	8.9	32.7	14.5	0.8	1.4
5	38.4	1.3	11.5	2.4	2.4	25	60.2	4.6	14.5	0.7	0.5
6	42.9	14.0	13.6	2.2	2.6	26	54.5	23.9	14.8	0.7	1.4
7	11.7	6.2	14.5	1.9	1.6	27	6.7	15.5	16.4	0.5	0.8
8	41.3	-2.0	12.4	1.8	3.0	28	20.9	-23.0	16.2	0.5	1.6
9	16.8	0.3	14.6	1.8	1.9	29	15.2	-8.0	12.4	0.4	0.6
10	8.2	-3.2	14.9	1.6	2.1	30	15.2	24.7	13.9	0.4	0.6
11	42.9	20.6	13.7	1.6	2.9	31	31.3	39.4	12.9	0.2	0.3
12	55.1	16.4	12.1	1.5	2.1	32	20.6	39.4	13.8	0.2	0.3
13	14.0	9.7	15.3	1.5	1.9	33	0.0	0.0	13.7	0.2	0.3
14	4.9	-8.8	15.5	1.5	1.4	34	25.5	0.3	10.0
15	-0.5	7.1	15.1	1.5	1.0	35	26.0	-3.6	11.4	2.9	...
16	12.2	26.7	16.0	1.5	0.8	36	12.9	-4.1	14.4	0.1	...
17	-4.7	5.0	15.3	1.3	2.3	37	5.3	12.5	14.9	2.6	...
18	17.3	-14.8	15.0	1.3	2.5	38	-20.5	45.3	10.2	0.1	...
19	30.0	3.0	8.9	1.3	3.3	39	-16.9	40.8	11.3	0.0	0.0
20	5.6	32.5	16.1	1.2	1.2						

^aRight ascension and declination offsets from NIRS 33 [$\alpha = 23^{\text{h}}15^{\text{m}}05.55^{\text{s}}$, $\delta=+59^{\circ}12'24.2''$, 1950.0].

The [H-K']-[J-H] diagram for all the point sources detected in all three wavelength bands is presented in Fig. 3. Plotted are 33 sources inside the $\sim 70''$ nebular region and 223 sources outside that have observed [H-K'] and [J-H] colors. Most of the sources outside the nebular region are assembled around an unredeemed main-sequence area, while the sources inside are spread over a much larger area in the large reddening direction and to the right of the reddening bands. There are 22 sources ($\sim 60\%$) inside the nebula, and 70 sources ($\sim 30\%$) outside, displaying infrared excesses. Note the sources outside are mainly situated in the zone of Herbig Ae/Be stars (Lada & Adams 1992) of intermediate masses ($2 - 10 M_{\odot}$) and T Tauri-like SEDs. The 16 sources (NIRS 1-16) inside the nebular region show typical characteristics of protostars

(Class I luminous sources, $[H-K'] > 1.5$ and $[J-H] > 0.7$, Lada & Adams 1992), while none outside do. Therefore, a cluster of young stars can be identified associated with the far infrared source IRAS 23151 in the nebular region.

Figure 4 shows the K' luminosity function (KLF) for the sources inside and outside the nebular region. It can be seen that KLF of the cluster sources peaks around magnitude 15, while that of the outside sources increase toward the faint magnitude limit. Note that the cluster sources are rather few in number and may not be given too much statistical significance. In general, we found 65%–70% of the cluster sources are brighter than magnitude 15, and only about 20% of sources outside are so.

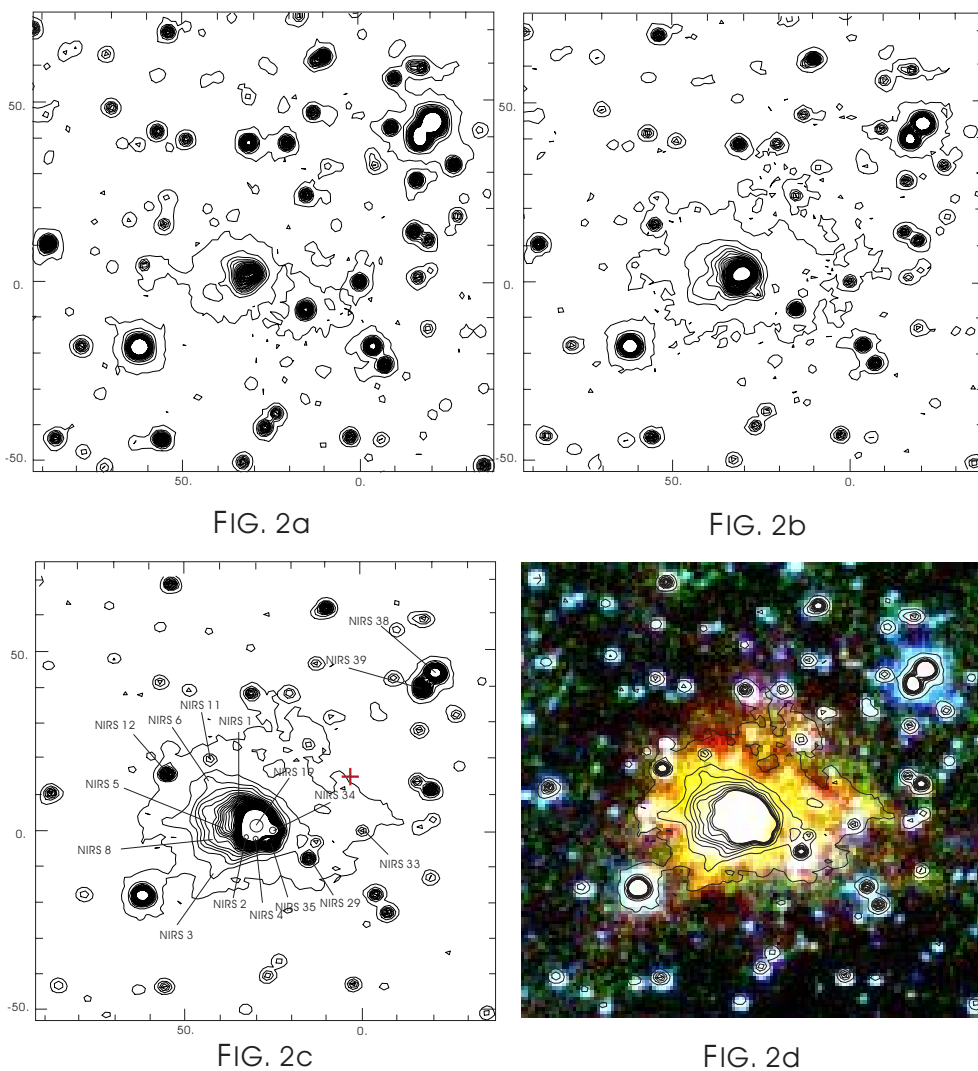


Fig. 2 Closer view of nebular area in IRAS 23151. The field of view is $130'' \times 130''$. (a) In the J band; (b) In the H band; (c) In the K' band; (d) JHK' log-scale color image. Axes are offset in arcseconds from the reference star NIRS 33 ($23^{\text{h}}15^{\text{m}}05.55^{\text{s}}$, $+59^{\circ}12' 24.2''$, [B1950.0]). The red cross in Fig. 2c marks the position of the radio emission peak in Miralles et al. (1994).

The color-magnitude diagrams (CMDs) of IRAS 23151 are presented in Fig. 5. Figure 5a shows seven sources with spectral types earlier than O9, and these are all cluster sources. The cluster sources are widely spread in the diagram, while the majority of the sources outside are assembled between A0 and K5 and near the main sequence line. Figure 5b has a similar appearance. There are five cluster sources with spectral types earlier than B2 and only two outside sources. The results suggest that the cluster sources tend to be not only younger, but also more massive than the sources outside. The difference between Figs. 5a and 5b may be noted. The difference between the two CMDs provides evidence of circumstellar dust emission in the K' band; the J magnitudes (Fig. 5b) will be less affected by circumstellar material, and so should more reliably reflect the mass estimation. Comparing Fig. 5b with Fig. 5a, we find that NIRS 19 is the only source with spectral type earlier than O9 in both, and similarly, the sources NIRS 8, 11, 12, and 29 have about the same spectral types in the two figures. It is probable that the spectral types of these sources (NIRS 8, 11, 12, 19, and 29) are confirmable. Assuming they are main sequence stars, the results show that the five cluster sources (NIRS 4, 5, 8, 12, and 19) are high-mass YSOs, four (NIRS 2, 6, 11, 29) are intermediate-mass YSOs, and the others have solar masses.

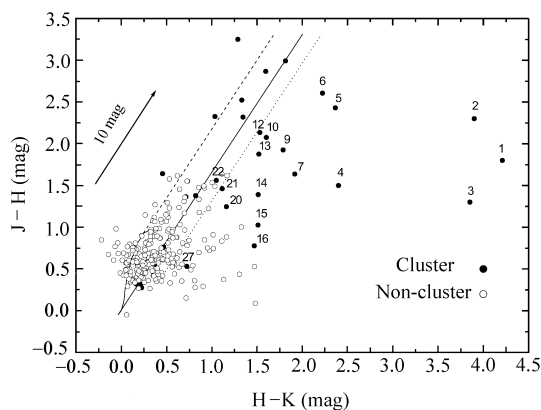


Fig. 3 JHK' color-color diagram for the point sources in IRAS 23151. The main sequence and giant branch are also shown as solid curves (Bessell & Brett 1988). The short-dashed line separates stars by shifting the reddening belt by an uncertainty in observed $[H-K']$ colors of 0.2 mag. A 10 mag visual extinction vector is also plotted for reference.

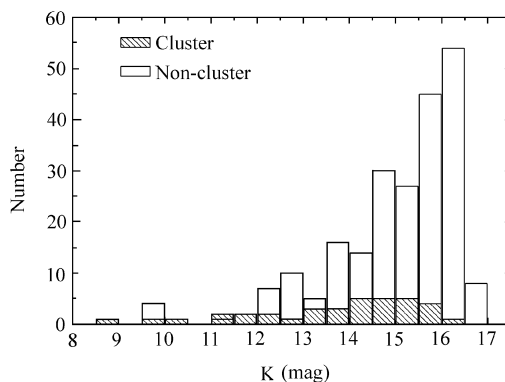


Fig. 4 K' luminosity function of point sources in IRAS 23151, 0.5 mag bins.

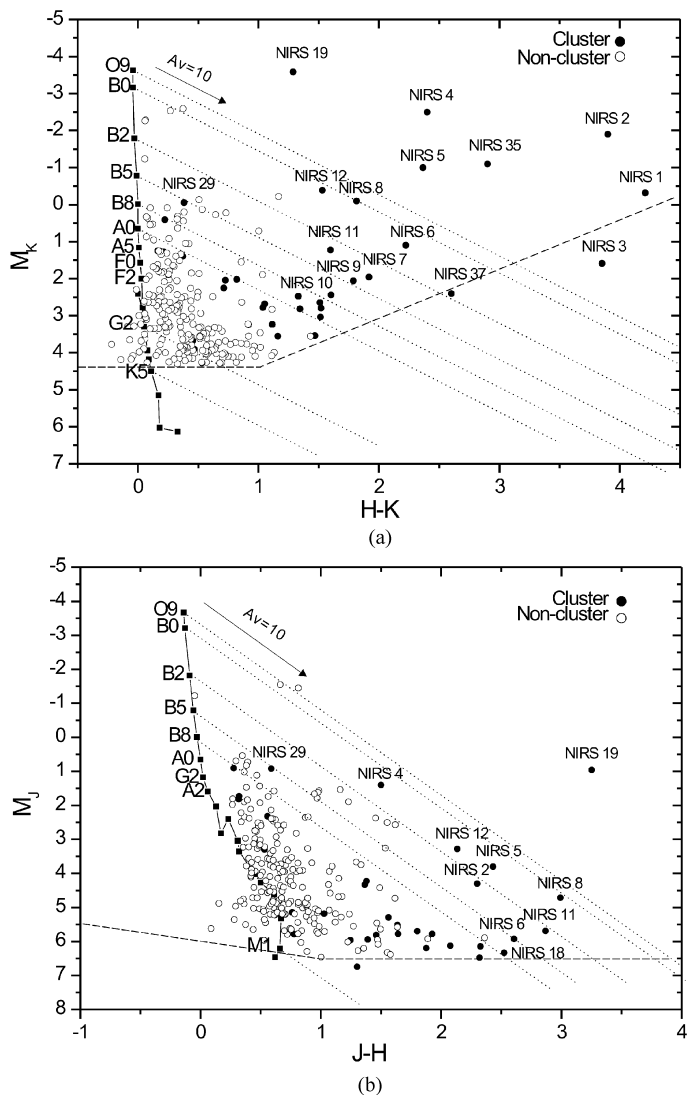


Fig. 5 Color-magnitude diagrams of point sources in IRAS 23151. The distance modulus of IRAS 23151 is $M=12.5$. The main sequence is marked by the solid curve (Porrás et al. 2000). The dashed lines show the detection limits. A 10 mag of visual extinction vector is also plotted for reference.

The H_2 line emission image of IRAS 23151 is shown in Fig. 6. Eight H_2 emission features are identified on the east and to the west of the infrared nebula. Their positions, fluxes, and morphologies are listed in Table 2. There is a large but very faint ‘V-type’ diffuse H_2 emission feature to the north of the cluster. The details of these features will be discussed in Sect. 4.3.

The K-band spectrum of NIRS 19 in IRAS 23151 is shown in Fig. 7. Main spectral features of young stars can be seen, such as HI ($2.166 \mu\text{m}$), H_2 ($2.034, 2.122, 2.223, 2.248 \mu\text{m}$), and CIV ($2.078 \mu\text{m}$). We regard a feature as “detected” if it is more than 3σ above the local continuum. The equivalent widths and fluxes measured for the $\text{Br}\gamma$, H_2 , and CIV lines are listed in Table 3.

Table 2 Positions and Flux Measurements of H₂ Emission in IRAS 23151

No	$\Delta\alpha^a$ ($''$)	$\Delta\delta^a$ ($''$)	Flux ($10^{-20}\text{W cm}^{-2}\mu\text{m}^{-1}$)	Aperture ^b ($''$)	Morphology
1.....	4.9	-8.8	10.52	2.0	Knot
2.....	9.5	5.0	245.93	25.0	Arc
3.....	26.5	37.0	4.91	2.0	Knot
4.....	37.5	4.0	5.54	2.0	Knot
5.....	37.0	0.5	17.99	3.0	Knot
6.....	39.5	-4.0	15.35	3.0	Knot
7.....	41.0	-6.5	6.51	2.0	Knot
8.....	50.2	-10.5	7.29	2.0	Knot
Diffuse	24.5	86.0	228.97	80.0	Diffuse

^a Offset origin is same as Table 1; ^b Aperture used in the H₂ flux measurement.

Table 3 Equivalent Widths and Fluxes of the Spectral Lines of NIRS 19

λ (μm)	Feature	EW(\AA)	Flux ($\times 10^{-17}\text{W m}^{-2}$)
2.248	H ₂ $v = 2 - 1\text{S}(1)$	1.6	1.5
2.223	H ₂ $v = 1 - 0\text{S}(0)$	3.0	2.7
2.166	Br γ	4.0	3.1
2.122	H ₂ $v = 1 - 0\text{S}(1)$	7.5	6.5
2.078	CIV	3.1	2.5
2.034	H ₂ $v = 1 - 0\text{S}(2)$	3.2	2.5

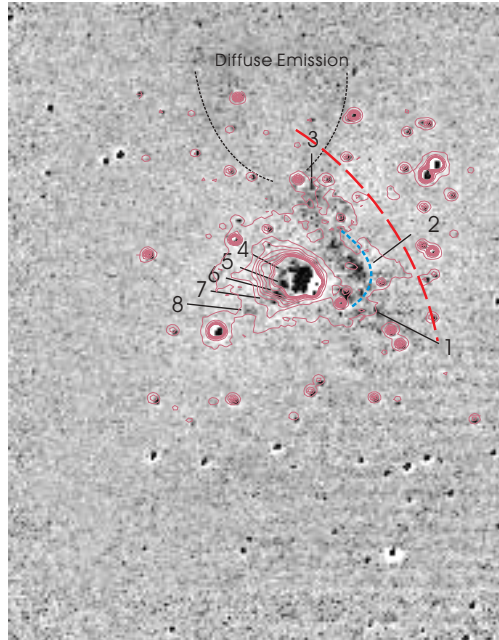


Fig. 6 H₂ line emission image of IRAS 23151 with the K-contour map of Fig. 2c superimposed. The field of view is $\sim 3' \times 4'$. The features of pure H₂ line emission are labelled. The blue and black dashed lines outline the bow-shaped H₂:2 emission and the large-scale diffuse emission to the north. The red dashed line represents the dark lane between the infrared and optical nebulae (see text).

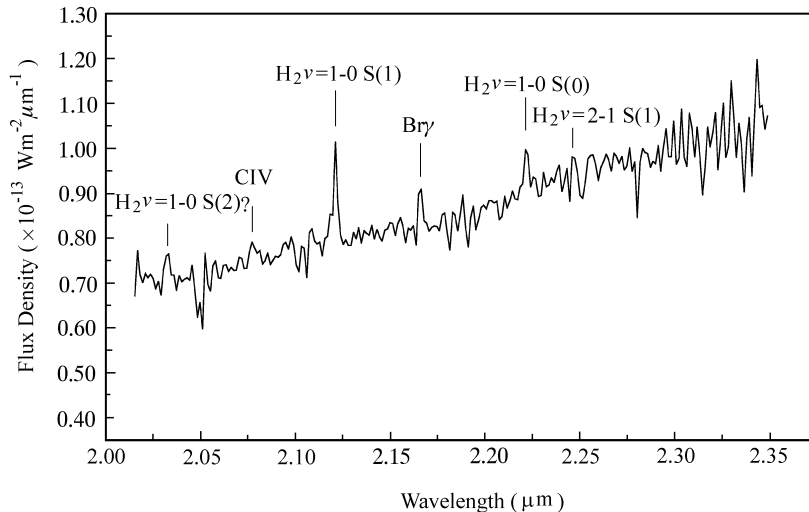


Fig. 7 Medium-resolution ($\lambda/\Delta\lambda \sim 500$) spectrum of NIRS 19 in IRAS 23151. All line emissions identified are indicated.

4 DISCUSSION

4.1 The Infrared Cluster

The near-infrared images reveal an embedded small cluster associated with the massive star formation source IRAS 23151. The extinction to the cluster is up to 15 mag, as estimated via the color-color diagram. As defined in this paper, 37 point sources are projected in the $\sim 70''$ cluster area associated with bright infrared nebula. Of the 37 point sources 22 ($\sim 60\%$) show large infrared excesses, indicating active star formation occurring in the area.

It is interesting to explore the age of clusters with massive young stars. It has been shown that the proportion of infrared excess sources in a stellar population could depend on the evolutionary stage (Lada & Lada 1995; Lada et al. 1996 and references therein). In the IRAS 23151 cluster, this proportion is very close to the values for the clusters in NGC 1333 (61%; $\sim 10^6$ yr, Lada et al. 1996) and in Taurus (50%; $1 - 2 \times 10^6$ yr, Kenyon & Hartmann 1995). Furthermore, there are several bright blue stars in Fig. 1a around the bright nebula which could be foreground stars. If these are excluded, then the proportion of infrared excess sources in the cluster will be raised to $\sim 74\%$, which would make the IRAS 23151 cluster as young as $\sim 10^6$ yr. According to the model of Haisch et al. (2001), the age of the IRAS 23151 cluster can be estimated to be about 2.5×10^6 yr, which can be regarded as an upper limit. Another way to estimate the age of the IRAS 23151 cluster may be by outflow activity, which is generally associated with the earliest stages of stellar evolution (i.e., the first 10^5 years, Lada et al. 1996). It is known that the largest radius of CO outflow in IRAS 23151 is $\sim 20''$, and the highest velocity of the outflow emission is 70 km s^{-1} ($V_{\text{LSR}} = -54.4 \text{ km s}^{-1}$) (Wouterloot et al. 1989). This way we can obtain a lower bound of the cluster age of $\sim 2.2 \times 10^5$ yr.

As stated above, five sources (NIRS 4, 5, 8, 12, and 19) in the cluster are high mass YSOs, four sources (NIRS 2, 6, 11, 29) are intermediate-mass YSOs, and the other sources have solar-

size masses. Considering our detection limit is $0.65M_{\odot}$ (see the CMDs in Fig. 5), we estimate the total stellar mass of the cluster to be $92M_{\odot}$ on setting the masses of the massive, intermediate-mass, solar-type stars to be $10M_{\odot}$, $5M_{\odot}$, and $0.8M_{\odot}$, respectively. The surface density of the cluster is ~ 46 stars pc^{-2} , corresponding to a volume density of $180M_{\odot}\text{pc}^{-3}$, assuming spherical geometry. The overall star formation rate is then $\psi_{\text{SF}} \approx 9.2 \times 10^{-5}M_{\odot}\text{yr}^{-1}$. This rate is approximately twice as large as the overall star formation rates derived for the embedded cluster IC 348 ($\approx 4 \times 10^{-5}M_{\odot}\text{yr}^{-1}$) (Lada & Lada 1995) and NGC 1333 ($\approx 4.5 \times 10^{-5}M_{\odot}\text{yr}^{-1}$) (Lada et al. 1996).

In Fig. 2c, the eight point sources located in the bright nebular core (NIRS 1, 2, 4, 5, 8, 19, 34 and 35) are numbered. NIRS 1 shows the largest infrared excess in the cluster, which indicates it is an extremely young source. NIRS 2, 4, and 5 are bright in the K' band and also have large infrared excesses. NIRS 19 is the brightest source in the K' band, with $K' = 8.9$ mag. NIRS 35 is red and is not detected in the J band. NIRS 19 is the only source in the cluster with spectral type earlier than O9 in Fig. 5b. It is spatially located in the center of the nebular core, and should be the dominant source of the nebular emission and also a major contributor of the far-infrared luminosity of IRAS 23151. NIRS 8 corresponds to the bright part in the southeast of the nebular core, and has spectral type B0 in both CMDs. Thus, NIRS 8 may also be a massive star in the cluster.

NIRS 34 is detected in neither J nor H. The fact may imply that NIRS 34 is embedded much more deeply in the molecular core. It can be seen in Fig. 1a that NIRS 34 is located in the reddest part of the bright nebular core. Considering NIRS 34 is brighter than NIRS 1 in the K' band, we argue NIRS 34 is the youngest source in the cluster, although NIRS 1 has the largest infrared excess measured. The positions of the two H_2O maser spots detected in IRAS 23151 are $[23^{\text{h}}15^{\text{m}}08.413^{\text{s}}, +59^{\circ}12' 23.4'']$ and $[23^{\text{h}}15^{\text{m}}08.416^{\text{s}}, +59^{\circ}12' 23.64'']$, (1950.0, Tofani et al. 1995). These two maser spots coincide well with the near infrared point source NIRS 34, $[23^{\text{h}}15^{\text{m}}08.7^{\text{s}}, +59^{\circ}12' 24.5'']$. Using the “nearest neighbor” criterion (Testi et al. 1994, 1998), we can identify NIRS 34 as the powering source of the H_2O masers in IRAS 23151. This implies that NIRS 34 is also a very young massive star.

The CO outflow found in IRAS 23151 is centered on the bright nebular core (Wouterloot et al. 1989). Nevertheless, the identification of the driving source for the outflow is not straightforward, since several bright infrared sources are located in the core, and the driving mechanism for outflows in cluster region is uncertain. Based on the near-infrared imaging and photometry, we propose that NIRS 19 is a source associated with the massive molecular outflow. With its youthful and massive nature and its powering of the H_2O masers, NIRS 34 is also a likely driving source for the outflow.

4.2 The Infrared Nebula

The infrared nebula in IRAS 23151 consists of a bright nebular core surrounded by diffuse nebulosity. There are eight point sources, NIRS 1, 2, 4, 5, 8, 19, 34 and 35, detected in the nebular core, and two red sources NIRS 3 and 6, are found near the southeast and northeast edge (Fig. 2c). All the point sources could be associated with the infrared nebula and contribute to the nebular emission. Among these sources, NIRS 19 is the NIR emission peak and should be one of the dominant sources in the nebula. It should be noted that, under the current resolution, a few point sources identified in the bright nebula may be just nebular knots, although we take all of them as point sources in this paper.

Infrared nebula around young stars is one of important indicators of star forming activity

and environment. In IRAS 23151, three nebular juts are seen to the east and southeast of the bright central core; the juts to the right (east) and pass through NIRS 3 are relatively redder, while the jut through NIRS 8 is bluer, as seen in the J and H contours in the main SE nebular extension. The feature seems to outline a cavity structure from the central core along the SE direction. The infrared nebula also displays redder colors toward the outer layer, especially in the northwest direction. This property implies the infrared cluster and nebula in fact burst inside the dense cloud core, with denser cloud material outside the cluster region forming a cocoon structure.

To the northwest of the infrared nebula $\sim 2'$ is an optical nebula (Fig. 1b). Two bright visible sources, NIRS 38 and 39 (see Fig. 2c; and Table 1 for the photometric data), are found in the center of the optical nebula. We suggest the two brilliant stars are the exciting source of the optical nebula. Figure 1a shows some very red point sources detected between the infrared nebula and the optical nebula. A bow-shaped H_2 emission feature and two knots are found in the field. Following the cocoon nebular structure discussed above, there could be a dense lane of cloud material between the infrared and optical nebulae. The orientation of the lane is in the NE-SW direction, and we argue below that the dark lane may affect the direction of the CO outflows in the field.

In the CS (2–1) survey of IRAS sources by Bronfman et al. (1996), IRAS 23151 is attributed to sources associated with an ultra-compact (UC) HII region, based on spectral characteristics between $12\ \mu\text{m}$ and $100\ \mu\text{m}$. Although no continuum emission is seen at $3.5\ \text{cm}$ in the VLA map of Tofani et al. (1995), Miralles et al. (1994) found a radio source $\sim 30''$ to the northwest of IRAS 23151 position in their $2\ \text{cm}$ and $6\ \text{cm}$ VLA observations. Miralles et al. (1994) suggested that the dominant source of luminosity is a very young massive star that has not yet produced a detectable HII region, or there are large-scale inhomogeneities in the gas, causing the separation between the radio continuum and far-infrared peaks. In the NIR images, we could identify a very red point source, NIRS 37, associated with the radio source of Miralles et al. (1994). On the other hand, Beuther et al. (2002) detected $1.2\ \text{mm}$ dust continuum emission at the position of IRAS 23151. Wouterloot et al. (1989) also reported (Chini, private communication) detection of a $230\ \text{GHz}$ ($1.3\ \text{mm}$) source there. The near-infrared observations show that the brightest source, NIRS 19, is coincident with the IRAS position and should contribute much to the far infrared luminosity. By the evidence of dense dust envelope and surrounding ionized gas (see Sect. 4.4), NIRS 19 must be a very young massive star. The UC HII region around NIRS 19 could be comparative small in size and strongly self-absorbed at centimeter (cm) wavelengths, and can only be detected by dust continuum emission. Thus, the characteristics above of NIRS 19 is consistent with those of the earliest stage of high mass protostellar objects, such as high luminosity, strong dust emission, and very weak or undetectable free-free emission at cm wavelengths (Beuther et al. 2002). Therefore, NIRS 19 could be the ionizing source of the UC HII region of IRAS 23151.

Recent studies showed that H_2O masers can be present in the earliest evolutionary phase of a high mass protostar, even before the onset of an UC HII region (Palla et al. 1993; Codella et al. 1994). H_2O masers and UC HII regions, although generally found in the same star forming region, are not necessarily closely related to each other, and the powering sources of HII region and maser radiation have to be searched for in distinct objects at different evolutionary phases (Forster & Caswell 1989; Tofani et al. 1995; Jenness et al. 1995; Hofner & Churchwell 1996). The near infrared images improve our understanding of the star formation environment in IRAS 23151. Three distinct massive point sources, at least, can be identified in the

cluster area. NIRS 19 is the brightest near infrared source of the cluster, associated with dense dust envelope and powering an undetected UC HII region. NIRS 37 is located in the dark lane and is exciting an UC HII region. NIRS 34 is also located in the cluster center near NIRS 19, powering the H₂O masers but with no evidence of an UC HII region.

4.3 The H₂ Emission

There are eight H₂ emission features discovered in the field of IRAS 23151. These H₂ emission features are mainly spread out to the east and west of the nebular core. H₂:2, morphologically bow-shaped to the west, is primarily composed of four sub-knots. The knots H₂:1 and 3, are found at either side of the bow and are diffuse in appearance. A relatively good alignment can be seen for the knots H₂:4, 5, 6, 7, and 8, along the NW–SE direction; H₂:4 is located near NIRS 1. The intensity of the knots gets gradually weaker from H₂:4 to 8. These five knots seem to outline an H₂ flow and may imply that NIRS 1 is the headstream of the flow.

The scattered and non-axisymmetric distribution of the H₂ features around the cluster indicate the existence of multiple outflows driven by several sources. It is known that collisional excitation in shocked gas is the dominant H₂ emission mechanism in protostellar flows. On the other hand, H₂ excitation through UV fluorescence has been noticed, in particular, near hot young stars. We suggest that the flow of the knots H₂:4–8 results from collisional excitation and is driven by NIRS 1, an extremely young star with the largest infrared excess in the cluster. This flow shows a periodicity of multiple outbursts. Assuming the velocity of the H₂ flows is 100 km s⁻¹ (Lee et al. 2000; Bally et al. 2002), we can estimate the timescales from H₂:4 to 5, 5 to 6, 6 to 7, and 7 to 8 to be ~ 800 yr, ~ 800 yr, ~ 700 yr and ~ 1700 yr, respectively.

We take the diffuse knot H₂:2 to be UV fluorescent. In fact, the H₂ feature follows the edge of the infrared nebula, probably marking the interaction surface of the dense lane. NIRS 19 is suggested to be the powering source of the H₂ emission for the following reasons. Morphologically, NIRS 19 is at the corresponding position of the bow-shaped feature; NIRS 19 is the brightest source in the cluster and powering UC HII region, so that there could be strong UV photons driving the large-scale H₂ emission. The H₂ feature provides further constraint on the density structure of the region. There must be an optically thin channel or cavity to allow enough leakage of UV photons, and the scale of H₂:2 suggests a large opening angle of the westward cavity.

For the knots H₂:1 and 3, it is not easy to identify the excitation mechanism by morphology. The two knots are a little diffuse and may also indicate the interaction surface. There is also a possibility that H₂:1 and 3 mark two flow streams to the north and to the southwest. The large diffuse ‘V-type’ feature to the north may imply a cavity route in the cloud core. This kind of large-scale diffuse H₂ emission has recently been observed in the star-forming regions S255 IR and AFGL 5157 (Howard et al. 1997; Miralles & Salas 1997; Chen et al. 1999). The excitation mechanism could be UV fluorescence, which usually leads to diffuse emission on a larger scale (e.g., Gatley et al. 1987).

There is no spatial relationship between the H₂ emission detected and the CO molecular outflow in the region. The CO outflow was observed in the NE-SW direction (Wouterloot et al. 1989), while the H₂ emission features are detected to the east and to the west of the IRAS 23151 position. This picture makes it rather difficult to understand the driving of the CO outflow. It is now believed that CO outflow is an integral result of optical and near infrared mass flows. Assuming an E–W outflow of IRAS 23151 in the near infrared, we can only imagine the CO outflow has been curved to the NE–SW direction by the dark lane to the west of the

cluster. High resolution mapping is necessary to reveal the detailed structure of molecular outflow in the region.

4.4 The Massive Central Star

In our spectrometry observations, the slit of spectrometer was centered on the K-band peak of IRAS 23151, NIRS 19. $\text{Br}\gamma$ and H_2 emissions are found in the spectrum, which are frequently seen in the spectra of YSOs (Greene & Lada 1996; Porter et al. 1998; Ishii et al. 2001). The $2.166\ \mu\text{m}$ $\text{Br}\gamma$ line is the only hydrogen line expected in this wavelength region. The line emission is generally thought to occur in stellar wind close to stars (Ishii et al. 2001 and references therein). In the K-band spectroscopic study of YSOs, $\text{Br}\gamma$ emission shows correlation with the luminosity, rather than the SED of the sources (Greene & Lada 1996; Ishii et al. 2001), indicating that the emission is closely associated with the mass of YSOs. On the other hand, H_2 emission clearly depends on the SEDs from Class I to Class II (Greene & Lada 1996; Ishii et al. 2001). H_2 emission is mainly detected in the Class I YSOs, but rarely detected in the Class III. This fact indicates that the emission may be closely associated with circumstellar envelopes.

To infer emission mechanism, we calculate the ratio of H_2 1–0 S(1)/ 2–1 S(1) lines of NIRS 19. Generally, line ratios of $\sim 10:1$ are observed in shocked regions, and $\sim 2:1$ in the photodissociation regions (PDRs) (Shull & Bechwith 1982; Martini et al. 1999). The line ratio in NIRS 19 is found to be $\sim 5:1$, supporting the idea of shock excitation. Therefore, the $\text{Br}\gamma$ and H_2 emissions in the K-band spectrum show properties of envelope, ionized gas and shocks in the circumstellar environment of NIRS 19.

The $2.078\ \mu\text{m}$ CIV line is found on the K-band spectrum of NIRS 19, which is usually apparent in mid-O and late-O type stars (Hanson, Conti & Rieke 1996). Both CIV and $\text{Br}\gamma$ in emission without NIII and HeI lines may imply O7–O8 spectral type YSOs. This range of spectral types corresponds to effective temperatures of 41,010 to 38,450 K (Vacca, Garmany, & Shull 1996). Adopting $\log L/L_\odot$ of 5.404–5.235 for O7–O8 star (cf. table 5 of Vacca et al. 1996), the source NIRS 19 could have a mass of $30 M_\odot$, and an estimated age of less than 1×10^6 yr, according to its position in the theoretical H-R diagram (Watson et al. 1997a,b). To summarize, with the O9 spectral type estimated by the infrared CMDs, NIRS 19 should be a massive young star of $20 \sim 30 M_\odot$.

It is remarkable that five high mass stars (NIRS 4, 5, 8, 12, 19) and four intermediate-mass stars (NIRS 2, 6, 11, 29) were found in the IRAS 23151 cluster. If it is true, IRAS 23151 cluster may indicate a rare example of burst of massive stars. The uncertainty of our mass estimation is $\sim 30\%$ from the 0.1 mag photometric accuracy. Besides the near-infrared CMDs method, several lines of evidence show the clustered massive young stars. The separated H_2O maser in the region indicates the presence of massive stars, and the UC HII regions detected in mm- and cm-wave observations also display high mass ionizing sources. Furthermore, the massive molecular outflow in IRAS 23151 ($200 M_\odot$, Wouterloot et al. 1989) really need massive driving sources.

The bolometric luminosity of the massive stars in IRAS 23151 cluster, however, seems to be much higher than the IRAS luminosity of $3.9 \times 10^4 L_\odot$ measured toward the field. If we take the brightest near infrared source NIRS 19 as an O7–O9 ZAMS star, its luminosity alone would be $2.535 \sim 1.151 \times 10^5 L_\odot$, much larger than the far infrared luminosity. This difference may indicate that, in the specific environment of high mass star formation, significant stellar luminosity could escape in the near infrared wavelength. In the young stellar cluster S87 (Barsony 1989;

Chen et al. 2003), there are also massive molecular outflow, H₂O maser and UC HII regions detected in mm- and cm-wavelengths. Barsony (1989) has estimated by the radio observations a massive star of $20 M_{\odot}$ as the powering source, corresponding to a ZAMS stellar luminosity of $\sim 1.151 \times 10^5$. This luminosity is also much larger than the IRAS luminosity of 3.5×10^4 toward the S87 region.

5 CONCLUSIONS

We have obtained near-infrared images and K-band spectroscopy of the massive star forming region IRAS 23151. The images reveal an embedded massive cluster associated with infrared nebula and H₂ emission. The main results can be summarized as follows.

A total of 37 near-infrared sources are detected in association with infrared nebula in the $\sim 70''$ (~ 1 pc) region of IRAS 23151; 22 ($\sim 60\%$) of these show infrared excesses. The near infrared properties allow us to identify five high mass and four intermediate-mass YSOs in the cluster. The age of the cluster in IRAS 23151 is suggested to be less than $\sim 10^6$ yr.

NIRS 1 shows the largest infrared excess and may excite H₂ flows. NIRS 19 is the brightest source in the K' band and is associated with dense dust envelope and UC HII region. NIRS 34 may be the youngest source associated with H₂O masers in the region. NIRS 37 is identified as the near infrared counterpart of the UC HII region in the dark lane.

Eight H₂ emission features are discovered in the region. The scattered and non-axisymmetric distribution of the H₂ features could indicate multiple outflow activity. The knots H₂: 4–8 seem to be aligned in the eastern side of the nebula, probably driven by NIRS 1. H₂: 2 displays a bow-shaped diffuse structure to the west of the nebula; it could result from UV fluorescence of NIRS 19.

Eight young stars are found in the bright infrared nebular core of IRAS 23151. The near infrared images seem to outline a dark lane of cloud material oriented in the NE–SW direction westward the infrared nebula. The infrared nebula displays redder colors toward the outer layer, implying the infrared cluster and nebula burst inside a cocoon cloud core. A cavity structure can be identified in the SE and west directions by the SE bluer nebular extension and the diffuse bow-shaped H₂ emission feature.

Br γ , H₂, and CIV emissions are found on the K-band spectrum of NIRS 19, indicating the presence of envelope, ionized wind and shock. The spectral type of NIRS 19 is suggested to be O7–O9, and the mass estimated to be $20 \sim 30 M_{\odot}$ with an age of less than 1×10^6 yr.

Acknowledgements This work is supported by the National Natural Science Foundation of China under Nos. 10133020 and 10273022, and Ministry of Science and Technology G19990754.

References

- Barsony M., 1989, ApJ, 345, 268
- Bessell M. S., Brett J. M., 1988, PASP, 100, 1134
- Beuther H., Schilke P., Menten K.M., et al., 2002, ApJ, 566, 945
- Bronfman L., Nyman L.-A., May J., 1996, A&AS, 115, 81
- Cesaroni R., Felli M., Walmsley C. M., 1999, A&AS, 136, 333
- Chen Y. X., Zheng, X. W., Yao, Y. Q., Yang, J., & Sato, S., 2003, A&A, 401, 185
- Chen Y.-F., Yao Y.-Q., et al., 1999, AJ, 117, 446
- Codella C., Felli M., Natale V., Palagi F., Palla F., 1994, A&A, 291, 261

- Felli M., Palagi F., Tofani G., 1992, *A&A*, 255, 293
Fernandes A. J. L., Brand P. W. J. L., 1995, *MNRAS*, 274, 639
Forster J. R., Caswell J. L., 1989, *A&A*, 213, 339
Gatley I., Hasegawa T., Suzuki H. et al., 1987, *ApJ*, 318, L73
Greene T. P., Lada C. J., 1996, *AJ*, 112, 2184
Haisch K. E., Jr., Lada E. A., Lada C. J., 2001, *ApJ*, 553, L53
Hanson M. M., Conti P. S., Rieke M. J., 1996, *ApJS*, 107, 281
Hodapp K. W., 1994, *ApJS*, 94, 615
Hofner P., Churchwell E., 1996, *A&AS*, 120, 283
Howard E. M., Pipher J. L., Forrest W., 1997, *ApJ*, 481, 327
Hunt L. K., Mannucci F., Testi L. et al., 1998, *AJ*, 115, 2594
Ishii M., Nagata T., Nagata T., Sato S. et al., 2001, *AJ*, 121, 3191
Jenness T., Scott P. F., Padman, R., 1995, *MNRAS*, 276, 1024
Kenyon S. J., Hartmann L., 1995, *ApJS*, 101, 117
Lada C. J., Adams F., 1992, *ApJ*, 393, 278
Lada C. J., Alves J., Lada E. A., 1996, *AJ*, 111, 1964L
Lada E. A., Lada C. J., 1995, *AJ*, 109, 1682
Martini P., Sellgren K., DePoy D. L., 1999, *ApJ*, 526, 772
Miralles M. P., Rodríguez L. F., Scalise E., 1994, *ApJ*, 92, 173
Miralles M. P., Salas L., 1997, *ApJ*, 488, 749
Okumura S., Nishihara E., Watanabe E., Mori A., Kataza H., Yamashita T., 2000, *PASJ*, 52, 931
Palla F., Cesaroni R., Brand J., et al., 1993, *A&A*, 280, 509
Porrás A., Gruz-Gonzalez I., Salas L., 2000, *ApJ*, 573, 221
Porter J. M., Drew J. E., Lumsden S. L. 1998, *A&A*, 332, 999
Scalise E. Jr., Rodríguez L. F., Mendoza-Torres E., 1989, *A&A*, 221, 105
Shull J. M., Bechwith S., 1982, *ARA&A*, 20, 163
Testi L., Felli M., Persi P., Roth M., 1994, *A&A*, 288, 634
Testi L., Felli M., Persi P., Roth, M., 1998, *A&AS*, 129, 495
Tofani G., Felli M., Taylor G. B., Hunter T. R., 1995, *A&AS*, 112, 299
Vacca W. D., Garmany C. D., Shull J. M., 1996, *ApJ*, 460, 914
Wallace L., Hinkle K., 1997, *ApJS*, 111, 445
Watson A. M., Coil A. L., et al., 1997a, *ApJ*, 487, 818
Watson A. M., Hanson M. M., 1997b, *ApJ*, 490, L165
Wouterloot J. G. A., Henkel C., Walmsley C.M., 1989, *A&A*, 215, 131
Wouterloot J. G. A., Walmsley C. M., 1986, *A&A*, 168, 237
Wouterloot J. G. A., Walmsley C. M., Henkel C., 1988, *A&A*, 203, 367